

Med-Art: Diffusion Transformer for 2D Medical Text-to-Image Generation

Changlu Guo, Anders Nymark Christensen, and Morten Rieger Hannemose

Department of Applied Mathematics and Computer Science,
Technical University of Denmark, Kgs. Lyngby, Denmark
{chagu, anym, mohan}@dtu.dk

Abstract. Text-to-image generative models have achieved remarkable breakthroughs in recent years. However, their application in medical image generation still faces significant challenges, including small dataset sizes, and scarcity of medical textual data. To address these challenges, we propose Med-Art, a framework specifically designed for medical image generation with limited data. Med-Art leverages vision-language models to generate visual descriptions of medical images which overcomes the scarcity of applicable medical textual data. Med-Art adapts a large-scale pre-trained text-to-image model, PixArt- α , based on the Diffusion Transformer (DiT), achieving high performance under limited data. Furthermore, we propose an innovative Hybrid-Level Diffusion Fine-tuning (HLDF) method, which enables pixel-level losses, effectively addressing issues such as overly saturated colors. We achieve state-of-the-art performance on two medical image datasets, measured by FID, KID, and downstream classification performance. The project is available at <https://medart-ai.github.io>.

Keywords: Text-to-image · generative models · medical image generation.

1 Introduction

The emergence of diffusion models [11] has driven huge advancements in text-to-image generation, achieving unprecedented success in natural image synthesis. Proprietary models such as Imagen 3 [3], alongside open-source frameworks like Stable Diffusion [24], Hunyuan-DiT [18], and PixArt- α [6], have demonstrated remarkable capabilities in generating high-fidelity and diverse images. These models are trained on web-scale data, which contains little medical data, greatly limiting their ability to generate this out-of-the-box. Despite this, diffusion-based generative models hold significant potential in medical contexts, such as synthesizing rare diseases, enabling privacy-preserving data sharing, and improving medical education.

Recent studies have explored applications of diffusion models across diverse medical scenarios, including 3D vascular graph synthesis [26], iterative online image synthesis for mitigating class imbalance [17], and anatomically constrained

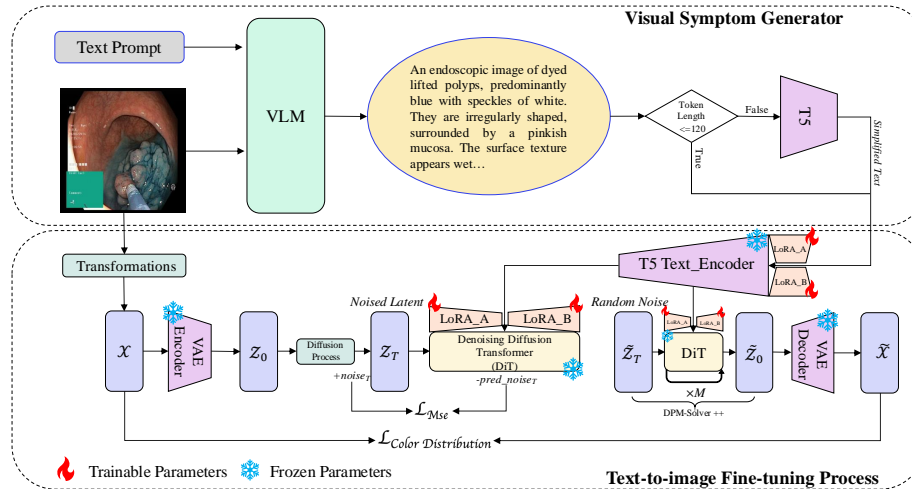


Fig. 1: The architecture of Med-Art (the parameters of DiT are shared)

generation using segmentation masks [15]. However, unlike the rapid advancements in natural image generation, research on medical domain-specific text-to-image diffusion models remains less explored. Existing methods, such as RoentGen [5], fine-tune Stable Diffusion to generate chest X-ray images but are constrained by their reliance on radiology-specific text prompts. For most other medical imaging modalities, such detailed textual descriptions are unavailable. For instance, Akrouf et al. [1] generate skin lesion images using only class labels as prompts. This constraint restricts the model’s ability to fully exploit the potential of text-to-image technology for medical image generation.

Therefore, the application of text-to-image within the medical domain still faces significant bottlenecks. This is largely due to strict privacy and ethical constraints that severely limit public access to medical images and their associated textual data. Furthermore, text connected to medical images is typically highly specialized, such as medical records, which require specialized knowledge to connect to images. Additionally, we observed that fine-tuning models pretrained on natural images can cause color oversaturation issues in color-sensitive 2D RGB modalities such as endoscopic and dermoscopic images.

To overcome these issues, we propose Med-Art, a framework designed to adapt and enhance text-to-image models for 2D medical image generation, improving fidelity, accuracy, and clinical applicability. Our main contributions are:

- This is the first work to leverage a vision-language model (VLM) [32] to generate high-quality, visually grounded natural image descriptions that resemble the language distribution seen during text-to-image model pretraining, thereby addressing the scarcity of medical textual data and enabling effective text-to-image fine-tuning.

- Based on the Diffusion Transformer (DiT) [23] model PixArt- α , we apply LoRA [13] to both the DiT module and text encoder, optimizing only a small subset of parameters. This enables the model to capture medical semantics and generate high-quality medical images from limited data.
- We propose a novel method to ensure color consistency by integrating the Diffusion Probabilistic Model Solver [21] into generative model fine-tuning. Generating images during training enables pixel-level loss computation.

Experimentally, Med-Art achieves state-of-the-art performance on two small-scale medical image datasets, significantly surpassing existing methods such as the Stable Diffusion series and PixArt- α , and also demonstrates superior downstream classification task performance.

2 Method

Med-Art is structured, as shown in Fig. 1. The Visual Symptom Generator (VSG) generates detailed visual text descriptions from the original medical images and prompts. These descriptions, combined with the transformed images (e.g., normalized), are used in the fine-tuning process to learn the relationship between visual representations and text.

2.1 Visual Symptom Generator (VSG)

In the medical domain, due to the specialized nature and privacy concerns, obtaining image descriptions with text annotations is challenging. Our VSG leverages the knowledge and multimodal capabilities of vision-language models to generate visual descriptions of medical images. Specifically, as shown in the upper part of Fig. 1, we use the LLaVA-Next [16] model to generate descriptions for medical images through prompts. This allows for the description of the visual appearance in a more natural language, which is better suited for the pretrained text-to-image models. To generate the corresponding visual symptom descriptions, we use the image and the following structured textual prompt:

Q: An/A {modality} image of {category}. Please describe the {modality} image of {category} using the following visual features: {visual features}. Start with ‘An/A {modality} image of {category}’ and ensure the description does not exceed 100 words.

Here {modality} represents the imaging modality of the dataset, such as dermoscopic for skin images; {category} refers to a specific category, and {visual features} denotes the corresponding visual features associated with the given modality. This information and examples of generated texts are in Table 1. The pre-trained DiT from PixArt- α is limited to 120-tokens, yet certain generated texts exceed this constraint, leading to information loss upon truncation; thus, we employ T5 [27] for text simplification, directly retaining texts within 120 tokens while prompting T5 with "simplify: {generated_text}" for longer texts to generate a concise 90-120 token version, ensuring information integrity.

Table 1: A single sample from both datasets, along with a simple caption, and a caption from the VSG, used for the text-to-image model.

Dataset	Kvasir	Skin lesions
Sample		
Modality	endoscopic	dermoscopic
Category	dyed lifted polyps	Melanoma
Visual features	specific color, shape, surrounding mucosa, surface texture, bleeding condition, and other relevant details	specific color, symmetry, border, shape, texture and dermoscopic patterns
Simple caption	An endoscopic image of dyed lifted polyps	A dermoscopic image of Melanoma
LLaVA-Next refined caption (VSG)	An endoscopic image of dyed lifted polyps, predominantly blue with speckles of white. They are irregularly shaped, surrounded by a pinkish mucosa. The surface texture appears wet and smooth. There is no active bleeding evident in the image.	A dermoscopic image of Melanoma shows a brownish-black irregularly shaped patch with a rough, granular texture and a wavy border. It has a central dark area with lighter satellite lesions and a radial streak pattern emanating from the central lesion. The background is a pale, translucent skin tone.

2.2 Text-to-image Fine-tuning Process

Training Procedure for PixArt- α PixArt- α builds upon conditional latent diffusion [28], using a pretrained encoder [8] to encode the input image x into a latent representation $z_0 = E(x)$. The model learns the conditional probability distribution $p(z_0|y)$, where y is the text describing the target image. During training, at each time step t (uniformly sampled from $\{1, \dots, T\}$), a noisy latent variable is generated as: $z_t = \sqrt{\bar{\alpha}_t}z_0 + \sqrt{1 - \bar{\alpha}_t}\epsilon$, where $\bar{\alpha}_t$ is the cumulative noise attenuation coefficient, and $\epsilon \sim \mathcal{N}(0, I)$ represents Gaussian noise. The conditional denoising network $\epsilon_\theta(z_t, t, \tau_\theta(y))$ is trained to predict ϵ , optimizing the objective:

$$\mathcal{L}_{\text{PixArt-}\alpha} := \mathbb{E}_{E(x), y, \epsilon \sim \mathcal{N}(0, I), t} [\|\epsilon - \epsilon_\theta(z_t, t, \tau_\theta(y))\|_2^2] \quad (1)$$

Here, $\tau_\theta(y)$ is the text embedding produced by a frozen text encoder (e.g., T5 [27]), which guides denoising and ensures consistency. The denoising network, built on DiT, integrates $\tau_\theta(y)$ with latent features $\phi(z_t)$ using cross-attention [30], enabling conditional generation.

LoRA To efficiently adapt text-to-image generation models to the medical domain, we integrate LoRA [13] into PixArt- α . Unlike previous methods that freeze the text encoder [6, 18], LoRA adjusts the text encoder to better handle medical

context, improving text embeddings. The updated text embeddings are expressed as: $\tau_{\theta+\Delta\theta}(y) = \tau_{\theta}(y) + \Delta\tau(y)$, $\Delta\tau(y) = W_A^{(T5)}W_B^{(T5)}y$, where $W_A^{(T5)} \in \mathbb{R}^{d \times r}$ and $W_B^{(T5)} \in \mathbb{R}^{r \times d}$ are low-rank matrices, with $r \ll d$, ensuring efficient updates with minimal additional parameters. In the denoising network DiT, LoRA is applied to key components, including attention mechanisms and feed-forward layers. For instance, the query matrix in the cross-attention mechanism is updated as: $W'_Q = W_Q + W_A^{(DiT)}W_B^{(DiT)}$, with similar updates for the key and value matrices. These adjustments enable better integration of medical text conditions into the latent space, enhancing both semantic consistency and detail accuracy. With these modifications, the denoising network in PixArt- α is redefined as:

$$\epsilon_{\theta+\Delta\theta}(z_t, t, \tau_{\theta+\Delta\theta}(y)) = \epsilon_{\theta}(z_t, t, \tau_{\theta+\Delta\theta}(y)) + \Delta\epsilon(z_t, t, \tau_{\theta+\Delta\theta}(y)) \quad (2)$$

where $\Delta\epsilon(z_t, t, \tau_{\theta+\Delta\theta}(y)) = W_A^{(DiT)}W_B^{(DiT)}\phi(z_t, t, \tau_{\theta+\Delta\theta}(y))$. The optimization objective is then reformulated as:

$$\mathcal{L}_{\text{Pixart-}\alpha+\text{LoRA}} := \mathbb{E}_{E(x), y, \epsilon \sim \mathcal{N}(0, I), t} [\|\epsilon - \epsilon_{\theta+\Delta\theta}(z_t, t, \tau_{\theta+\Delta\theta}(y))\|_2^2] \quad (3)$$

Hybrid-Level Diffusion Fine-tuning (HLDF) The fine-tuning described in the previous sections operates purely in the latent space, but is prone to generating images with highly saturated colors. To address this, we penalize deviations of the color distribution in pixel space. We minimize the difference in the mean (μ_c) and standard deviation (σ_c) of each color channel c between the input image x and the generated image \tilde{x} . The loss is defined as:

$$\mathcal{L}_{\text{color}} := \mathbb{E}_x \left[\sum_c \left(\|\mu_c(\tilde{x}) - \mu_c(x)\|_2^2 + \|\sigma_c(\tilde{x}) - \sigma_c(x)\|_2^2 \right) \right] \quad (4)$$

In order to compute this loss, we need to generate images during training. For this, we use classifier-free guidance [12] with a guidance weight of 4.5, and for sampling, we utilize the DPM-Solver++ [21], which enables the generation of high-quality images in 15–20 steps.

Even with this relatively small number of steps required, this remains a computationally and memory-intensive process to differentiate. To lower the required memory, at the cost of additional compute, we utilize gradient checkpointing [7]. However, we drastically lower the required computation and training time by adopting an interval optimization strategy, where we only compute the loss every N steps. The loss is then

$$\mathcal{L}_{\text{HLDF}} = \mathcal{L}_{\text{Pixart-}\alpha+\text{LoRA}} + \begin{cases} \frac{1}{M} \cdot \mathcal{L}_{\text{color}}, & \text{step} \equiv 0 \pmod{N} \\ 0, & \text{otherwise.} \end{cases} \quad (5)$$

Here, M denotes the number of steps employed by DPM Solver++ for image generation during training, where the default value is 20, and $\frac{1}{M}$ is the weight.

An endoscopic image of **dyed lifted polyps** shows a polyp with a specific blue-green color, indicating it has been dyed. The polyp has a round shape with a smooth surface texture. The surrounding mucosa appears normal with no signs of bleeding. The polyp is lifted and clearly visible, allowing for a thorough examination.



An endoscopic image of **ulcerative colitis** shows a reddened, inflamed mucosa with a patchy, irregular surface texture. The color is a mix of red and brown, with some areas appearing more inflamed than others. There are visible ulcers and bleeding, with blood oozing from the surface. The surrounding mucosa is also affected, with a mix of red and brown hues, indicating active inflammation. The image captures the severity of the condition and the need for medical intervention.



A dermoscopic image of **Melanoma**, showing a distinct brownish-black patch with irregular borders and a speckled, mottled texture. The lesion exhibits a starburst pattern with radial streaming and a halo of pinkish skin surrounding it.



A dermoscopic image of **Vascular Lesion** features a distinct red color, often with a slightly pinkish hue. The shape is typically round or oval with a flat or slightly raised surface. The texture appears as a fine, branching network of blood vessels, with a tree-like appearance. Dermoscopic patterns include a starburst-like structure with radial lines emanating from the center, a glomerular pattern resembling a cluster of grapes, and a reticular pattern with intersecting lines.



Real SD1.4 SD1.5 SDXL PixArt- α Med-Art Fast-DiT

Fig. 2: Samples of generated images: each row shows a text prompt and a corresponding image generated by different methods. Fast-DiT generates images using only class labels instead of text prompts. The images generated by the other methods contain unnaturally saturated colors and are less similar to the real image than the result of Med-Art.

3 Experiments

Datasets We evaluate the model on two datasets. The Kvasir dataset contains 8 gastrointestinal endoscopy classes with 1,000 images each [25]. The skin lesions dataset includes multiple diagnostic classes, e.g., common nevus (4,906 samples), melanoma (1,180), seborrheic keratosis (805), carcinoma (728), lentigo solaris (229), dermatofibroma (169), vascular lesion (160), and actinic keratosis (140) [9]. Both datasets are split 80/20 for training and testing per class.

Baselines We compare against state-of-the-art text-to-image diffusion models, including U-Net-based [29] models from the Stable Diffusion [28] family (SD1.4, SD1.5, and SDXL [24]), as well as Hunyuan-DiT [18] and PixArt- α . We LoRA fine-tune both the denoising network and the text encoder for all models, except for Hunyuan-DiT, which only supports LoRA fine-tuning for the denoising net-

Table 2: Performance of models **LoRA**-tuned with image text from VSG on two datasets (except Fast-DiT). Lower is better, best performance indicated in **bold**.

Model	Kvasir			Skin lesions		
	FID	KFD	KID	FID	HFD	KID
Fast-DiT	102.99	3.98	0.059	86.53	3.95	0.053
SD1.4	117.85	8.36	0.077	100.75	21.21	0.091
SD1.5	143.72	6.80	0.103	88.61	14.54	0.112
SDXL	125.28	7.20	0.091	103.37	26.04	0.070
PixArt- α	72.86	1.85	0.030	73.68	7.14	0.045
Med-Art	51.99	1.21	0.012	67.45	4.47	0.034

Table 3: The effect of different modules on the Kvasir dataset. Lower is better; best performance indicated in **bold**.

Method	FID	KFD	KID
Empty caption	59.12	12.33	0.036
Only simple caption	55.44	1.73	0.015
w/o HLDF (PixArt- α)	72.86	1.85	0.030
w/o LoRA on T5	63.10	1.26	0.018
Hunyuan-DiT [18]	143.26	15.82	0.087
with DoRA [19]	55.88	1.26	0.014
Med-Art (Ovis [22])	48.14	1.28	0.013
Med-Art	51.99	1.21	0.012

work. Finally, we compare to Fast-DiT [14], a class-conditional diffusion model, using the DiT-S/8 variant trained from scratch, conditioned on class labels.

Experimental Setup We train all models on a single A100 GPU using mixed-precision [23]. All models are trained to generate 512×512 images with a learning rate of 10^{-4} . The LoRA rank 8 and batch size 1. We train for 10 epochs on skin lesions and 15 epochs on Kvasir dataset. The pixel-level loss Eq. (4) is applied every $N = 500$ steps for the Kvasir dataset and every $N = 1500$ steps for the skin lesions dataset. A random subset of training images, matching the test set size (1600 for Kvasir and 1665 for skin lesions), is used to generate text prompts for test image synthesis.

Generative performance In addition to the Fréchet Inception Distance (FID) [10], we replace the Inception V3-based feature extractor with publicly available ViT models¹, pretrained on the Kvasir and the HAM10000 datasets, terming these variants “KFD” and “HFD” respectively. Additionally, we use Kernel Inception Distance (KID) [4], which enhances sensitivity for small datasets. Table 2 and Fig. 2 present the quantitative analysis and generated medical image examples from different models. For all models, Med-Art achieves the best performance across all metrics, except HFD. While PixArt- α ranks second, it suffers from severe color distortion, exhibiting oversaturation on the Kvasir dataset and even color deviation in skin lesion images. SD1.4 and SD1.5 typically produce overly smooth or distorted images, especially on the Kvasir dataset, while SDXL, although improving colors on Kvasir, still generates blurry and distorted skin images. Qualitatively, Fast-DiT struggles to generate features close to real pathological images. Med-Art generates highly realistic and high-quality medical images with superior color fidelity that closely resemble real medical imagery.

Table 3 illustrates the impact of different modules on Med-Art’s performance on the Kvasir dataset. Compared to the complete Med-Art model, removing VSG (using empty caption or simple caption), HLDF (equivalent to PixArt- α),

¹ mmuratarat/kvasir-v2-classifier, Anwarakh1/Skin_Cancer-Image_Classification

Table 4: Classification performance of models trained on synthetic or real data. Higher is better, best performance indicated in **bold**, second best in **gray**.

Training data	Method	Kvasir			Skin lesions		
		F1	BACC	AUC	F1	BACC	AUC
Synthetic	Fast-DiT	0.6492	0.6512	0.9256	0.5696	0.2287	0.7920
	SD1.4	0.5957	0.6450	0.9368	0.5177	0.3464	0.7840
	SD1.5	0.6192	0.6669	0.9622	0.5946	0.3039	0.8132
	SDXL	0.6830	0.7131	0.9683	0.3866	0.2721	0.7348
	PixArt- α	0.6291	0.6375	0.9730	0.5154	0.1680	0.7541
	Med-Art	0.8072	0.8119	0.9847	0.6090	0.3182	0.7994
Real	-	0.9361	0.9363	0.9962	0.7494	0.5080	0.9222

or LoRA on T5 all result in reduced performance. These findings indicate that the detailed, context-aware text prompts generated by VSG play a critical role in boosting model performance. Meanwhile, HLDF introduces only moderate computational overhead, increasing training time by 9% on the Kvasir dataset ($N = 500$, 12h14m \rightarrow 13h20m) and 6% on the skin lesions dataset ($N = 1500$, 9h9m \rightarrow 9h43m) in our experiments. More importantly, as demonstrated by the visual comparison between PixArt- α and Med-Art in Fig. 2, it significantly improves image quality—especially by reducing color distortion—without adding any extra time during the generation process. Considering the substantial gains in generation fidelity and clinical applicability (Table 3, Fig. 2), this trade-off is reasonable and worthwhile. Furthermore, fine-tuning the T5 encoder significantly enhances image generation; even without it, Med-Art outperforms the state-of-the-art Hunyuan-DiT, which fine-tunes only DiT. Although the recently introduced DoRA [19] demonstrates competitive performance, our experiments show that LoRA consistently outperforms DoRA on the Med-Art, reaffirming LoRA as the optimal choice for our setting. To demonstrate that our model generalizes to other prompts, we show results using prompts generated by Ovis [22], which achieved very similar results.

Classification performance Finally, to eliminate the influence of real data on classification performance, instead of using generated images for data augmentation [31], we fine-tune a classification model directly with them and evaluate its performance on the real test set. All images in the training set are used to generate texts and training data. We use a Vision Transformer [2], ViT-B/16, that is pretrained on natural images. We fine-tune using the AdamW optimizer [20] for five epochs with a learning rate of $2 \cdot 10^{-5}$. Table 4 shows that images generated by Med-Art enable the best classification performance on the Kvasir dataset. For the skin lesions dataset, while SD1.4 achieves the highest balanced accuracy (BACC) and SD1.5 obtains the best AUC, both models underperform Med-Art on the other two metrics. Taking into account all metrics, Med-Art demonstrates the best overall classification performance, not too far from the results obtained

using real data. This highlights Med-Art’s strong generative capability in producing category-specific samples that most resemble real images.

4 Conclusion

This study introduces Med-Art, which achieves state-of-the-art text-to-image generation in medical settings with limited numbers of images and text data by fine-tuning large-scale generative models on small medical image datasets, while also effectively mitigating color distortion in the generated images. Med-Art’s use vision-language models to overcome the lack of medical texts, furthermore implies that it can improve further upon future advancements in these.

References

1. Akrouf, M., Gyepesi, B., Holló, P., Poór, A., Kincső, B., Solis, S., Cirone, K., Kawahara, J., Slade, D., Abid, L., et al.: Diffusion-based data augmentation for skin disease classification: Impact across original medical datasets to fully synthetic images. In: *International Conference on Medical Image Computing and Computer-Assisted Intervention*. pp. 99–109. Springer (2023)
2. Alexey, D.: An image is worth 16x16 words: Transformers for image recognition at scale. *arXiv preprint arXiv: 2010.11929* (2020)
3. Baldrige, J., Bauer, J., Bhutani, M., Brichtova, N., Bunner, A., Chan, K., Chen, Y., Dieleman, S., Du, Y., Eaton-Rosen, Z., et al.: Imagen 3. *arXiv preprint arXiv:2408.07009* (2024)
4. Bińkowski, M., Sutherland, D.J., Arbel, M., Gretton, A.: Demystifying mmd gans. *arXiv preprint arXiv:1801.01401* (2018)
5. Bluethgen, C., Chambon, P., Delbrouck, J.B., van der Sluijs, R., Polacin, M., Zambrano Chaves, J.M., Abraham, T.M., Purohit, S., Langlotz, C.P., Chaudhari, A.S.: A vision–language foundation model for the generation of realistic chest x-ray images. *Nature Biomedical Engineering* pp. 1–13 (2024)
6. Chen, J., Yu, J., Ge, C., Yao, L., Xie, E., Wu, Y., Wang, Z., Kwok, J., Luo, P., Lu, H., et al.: Pixart- α : Fast training of diffusion transformer for photorealistic text-to-image synthesis. In: *International Conference on Learning Representations (ICLR)* (2024)
7. Chen, T., Xu, B., Zhang, C., Guestrin, C.: Training deep nets with sublinear memory cost. *arXiv preprint arXiv:1604.06174* (2016)
8. Esser, P., Rombach, R., Ommer, B.: Taming transformers for high-resolution image synthesis. In: *Proceedings of the IEEE/CVF conference on computer vision and pattern recognition*. pp. 12873–12883 (2021)
9. Hannemose, M.R., Sundgaard, J.V., Ternov, N.K., Paulsen, R.R., Christensen, A.N.: Was that so hard? estimating human classification difficulty. In: *International Workshop on Applications of Medical AI*. pp. 88–97. Springer (2022)
10. Heusel, M., Ramsauer, H., Unterthiner, T., Nessler, B., Hochreiter, S.: Gans trained by a two time-scale update rule converge to a local nash equilibrium. *Advances in neural information processing systems* **30** (2017)
11. Ho, J., Jain, A., Abbeel, P.: Denoising diffusion probabilistic models. *Advances in neural information processing systems* **33**, 6840–6851 (2020)

12. Ho, J., Salimans, T.: Classifier-free diffusion guidance. arXiv preprint arXiv:2207.12598 (2022)
13. Hu, E.J., Shen, Y., Wallis, P., Allen-Zhu, Z., Li, Y., Wang, S., Wang, L., Chen, W.: Lora: Low-rank adaptation of large language models. arXiv preprint arXiv:2106.09685 (2021)
14. Jin, C., Xie, S.: Fast-dit: Fast diffusion models with transformers. <https://github.com/chuanyangjin/fast-DiT> (2024)
15. Konz, N., Chen, Y., Dong, H., Mazurowski, M.A.: Anatomically-controllable medical image generation with segmentation-guided diffusion models. In: International Conference on Medical Image Computing and Computer-Assisted Intervention. pp. 88–98. Springer (2024)
16. Li, B., Zhang, K., Zhang, H., Guo, D., Zhang, R., Li, F., Zhang, Y., Liu, Z., Li, C.: Llava-next: Stronger llms supercharge multimodal capabilities in the wild. URL <https://llava-vl.github.io/blog/2024-05-10-llava-next-stronger-llms> (2024)
17. Li, S., Lin, Y., Chen, H., Cheng, K.T.: Iterative online image synthesis via diffusion model for imbalanced classification. In: International Conference on Medical Image Computing and Computer-Assisted Intervention. pp. 371–381. Springer (2024)
18. Li, Z., Zhang, J., Lin, Q., Xiong, J., Long, Y., Deng, X., Zhang, Y., Liu, X., Huang, M., Xiao, Z., et al.: Hunyuan-dit: A powerful multi-resolution diffusion transformer with fine-grained chinese understanding. arXiv preprint arXiv:2405.08748 (2024)
19. Liu, S.Y., Wang, C.Y., Yin, H., Molchanov, P., Wang, Y.C.F., Cheng, K.T., Chen, M.H.: Dora: Weight-decomposed low-rank adaptation. arXiv preprint arXiv:2402.09353 (2024)
20. Loshchilov, I.: Decoupled weight decay regularization. arXiv preprint arXiv:1711.05101 (2017)
21. Lu, C., Zhou, Y., Bao, F., Chen, J., Li, C., Zhu, J.: Dpm-solver++: Fast solver for guided sampling of diffusion probabilistic models. arXiv preprint arXiv:2211.01095 (2022)
22. Lu, S., Li, Y., Chen, Q.G., Xu, Z., Luo, W., Zhang, K., Ye, H.J.: Ovis: Structural embedding alignment for multimodal large language model. arXiv preprint arXiv:2405.20797 (2024)
23. Micikevicius, P., Narang, S., Alben, J., Diamos, G., Elsen, E., Garcia, D., Ginsburg, B., Houston, M., Kuchaiev, O., Venkatesh, G., et al.: Mixed precision training. arXiv preprint arXiv:1710.03740 (2017)
24. Podell, D., English, Z., Lacey, K., Blattmann, A., Dockhorn, T., Müller, J., Penna, J., Rombach, R.: Sdxl: Improving latent diffusion models for high-resolution image synthesis. arXiv preprint arXiv:2307.01952 (2023)
25. Pogorelov, K., Randel, K.R., Griwodz, C., Eskeland, S.L., de Lange, T., Johansen, D., Spampinato, C., Dang-Nguyen, D.T., Lux, M., Schmidt, P.T., et al.: Kvasir: A multi-class image dataset for computer aided gastrointestinal disease detection. In: Proceedings of the 8th ACM on Multimedia Systems Conference. pp. 164–169 (2017)
26. Prabhakar, C., Shit, S., Musio, F., Yang, K., Amiranashvili, T., Paetzold, J.C., Li, H.B., Menze, B.: 3d vessel graph generation using denoising diffusion. In: International Conference on Medical Image Computing and Computer-Assisted Intervention. pp. 3–13. Springer (2024)
27. Raffel, C., Shazeer, N., Roberts, A., Lee, K., Narang, S., Matena, M., Zhou, Y., Li, W., Liu, P.J.: Exploring the limits of transfer learning with a unified text-to-text transformer. *Journal of machine learning research* **21**(140), 1–67 (2020)

28. Rombach, R., Blattmann, A., Lorenz, D., Esser, P., Ommer, B.: High-resolution image synthesis with latent diffusion models. In: Proceedings of the IEEE/CVF conference on computer vision and pattern recognition. pp. 10684–10695 (2022)
29. Ronneberger, O., Fischer, P., Brox, T.: U-net: Convolutional networks for biomedical image segmentation. In: Medical image computing and computer-assisted intervention—MICCAI 2015: 18th international conference, Munich, Germany, October 5–9, 2015, proceedings, part III 18. pp. 234–241. Springer (2015)
30. Vaswani, A., Shazeer, N., Parmar, N., Uszkoreit, J., Jones, L., Gomez, A.N., Kaiser, Ł., Polosukhin, I.: Attention is all you need. *Advances in neural information processing systems* **30** (2017)
31. Yuan, Z., Fang, Z., Huang, Z., Wu, F., Yao, Y.F., Li, Y.: Adapting pre-trained generative model to medical image for data augmentation. In: International Conference on Medical Image Computing and Computer-Assisted Intervention. pp. 79–89. Springer (2024)
32. Zhang, J., Huang, J., Jin, S., Lu, S.: Vision-language models for vision tasks: A survey. *IEEE Transactions on Pattern Analysis and Machine Intelligence* (2024)